C 1.2 Ringleb

Marshall C. Galbraith*, Paul D. Orkwis†
University of Cincinnati, Cincinnati, OH, 45221

and

John A. Benek‡
U.S. Air Force Research Laboratory, Wright-Patterson Air Force Base, OH, 45433

I. Code Description

The solver relies a standard Discontinuous Galerkin discretization to achieve high-orders of accuracy. The spatial fluxes are approximated using the Roe approximate Riemann solver.[1] All integrals are evaluated analytically during a pre-processing stage using a symbolic manipulation package. The fluxes are computed from the conservative variables using a modal representation of the polynomials rather than a traditional nodal method. A more detailed description of the discretization and solver can be found in Refs. 2 and 3. The code is currently capable of up to 4^{th}-order polynomial approximations of the solution, which yields a 5^{th}-order accurate scheme. There is no inherent limitation that prevents polynomial approximations of higher order.

A linearized form of Euler equations is solved using an implicit Newtons method. The implicit system of equations of the Newtons method is solved using a flexible version of the GMRES iterative matrix solution algorithm, FGMRES.[4] A block ILU1[4] preconditioner is used for the FGMRES algorithm. The FGMRES algorithm was limited to 100 inner iterations. The FGMRES solver was converged to a residual below 10^{-14} on each Newton iteration. All calculations are in double precision.

Parallel capabilities are forthcoming.

II. Case Summary

The residual for the mean coefficient of the continuity equation, i.e. the density residual, from the first iteration was multiplied with 1×10^{-10} to yield the tolerance for a converged solution. The solution is also considered converged if the density residual drops below 5×10^{-15}. The solution was initialized to the analytical solution, and the solution was converge to a solution to steady state without a temporal term in the Euler equations when the analytical Ringleb solution was imposed on all boundaries. This is equivalent to $CFL = \infty$. A second set of simulations were performed where a slip wall boundary condition was imposed on the inner and outer walls. These simulations required a temporal term to achieve solutions where the the initial CFL number was set to 1, and was increased by a factor of 10 each Quasi-Newton iteration.

A summary of the exucation times and the average execution time of TauBench is shown in Table 1. The code was executed on an a machine with two 6 cores Intel i7 Xeon X5660 2.8 GHz processors. Only one core was used for all calculations.

*PhD Candidate, School of Aerospace Systems, AIAA Student Member.
†Professor of Aerospace Engineering & Engineering Mechanics, School of Aerospace Systems, AIAA Associate Fellow.
‡Director, Computational Sciences Center, Air Vehicles Directorate, Air Force Research Laboratory, AIAA Fellow.

Run	Execution Time (s)
1	7.815
2	7.674
3	7.698
4	7.962
5	7.669
6	7.712
7	7.691
8	7.953
9	7.676
10	7.668
Avg:	7.752

Table 1: Taubench Results

Timing of 100 right hand side (RHS) evaluations with 250,000 degrees of freedom (DOF) are summarized in Table 2. The RHS was evaluated on a uniform rectangular mesh. The solution was initialized to a free-stream flow with slip walls on the lower and upper surfaces. As the order of the polynomial approximation increased, the cell size of the mesh was reduced in order to maintain constant DOF. The 100 RHS evaluations were achieved by marching with a 4^{th}-order Runge-Kutta scheme 25 iterations.

Polynomial Order	Mesh Size	DOF	Work
0	500x500	250,000	6.24
1	250x250	250,000	2.70
2	167x167	251,001	2.58
3	125x125	250,000	3.32
4	100x100	250,000	4.92

Table 2: RHS Timing

III. Meshes

The DG solver is formulated for structured meshes. These meshes can be generated using any traditional mesh generator. After reading the mesh coordinates, the solver generates cell local polynomial representations, $(x(\xi,\eta), y(\xi,\eta))$, of the cell coordinates. The geometric polynomial mapping of the cell coordinates is formulated as a sum involving the same test functions, ψ, as used in the DG discretization of the governing equations. Hence,

$$\begin{aligned} x(\xi,\eta) &= \sum_{i}^{N_g}\sum_{j}^{N_g} x_{ij}\psi_{ij}(\xi,\eta) \\ y(\xi,\eta) &= \sum_{i}^{N_g}\sum_{j}^{N_g} y_{ij}\psi_{ij}(\xi,\eta) \end{aligned} \tag{1}$$

where x_{ij} and y_{ij} are the coefficients of the expansion, and $\psi_{ij}(\xi,\eta) = P_i(\xi)P_j(\eta)$, where $P_i(\xi)$ are the Legendre polynomials. The coefficients are found by equating the expansion with the associated cell nodal

values. The process is repeated for the y coordinate to obtain the final polynomial mapping of the cell. Additional points are required to establish the polynomial representation as shown for a quadratic cell in Fig. 1b. This implies that the grid must consist of $N_g n+1$ points along a coordinate line to generate n cells with a geometric mapping of order N_g along that line.

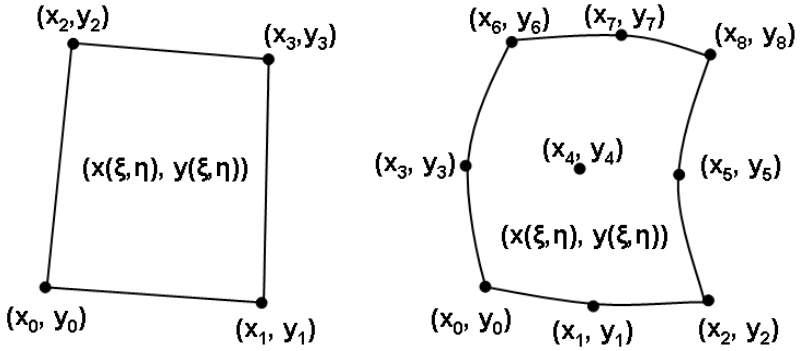

(a) Linear cell (b) Quadratic cell

Figure 1: Nodal and modal representation of cells.

The meshes provided by the workshop were used for this calculation. The mesh sizes used for the calculations are summarized in Table 3.

2x6	4x12	8x24	16x48	32x96

Table 3: Mesh Sizes Used for the Calculations

IV. Results

A. Ringleb Equation Walls

The convergence rate of three types of the L_2-error options are shown in Fig. 2. The convergence rate of the solution achieves the expect $O\left(h^{P+1}\right)$. L_2-errors vs. Work are shown in Fig. 3. With few exceptions, a higher degree polynomial achieves lower L_2-errors with less work. The convergence history of the Newton solver for the different meshes is shown in Fig. 4. The solution diverged on all meshes for $P = 0$.

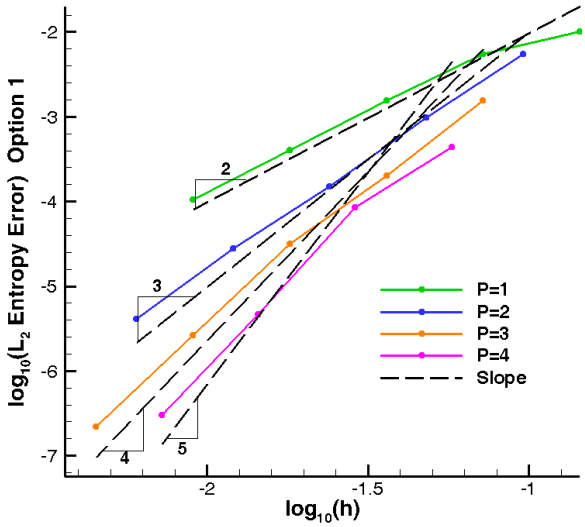

(a) Option 1

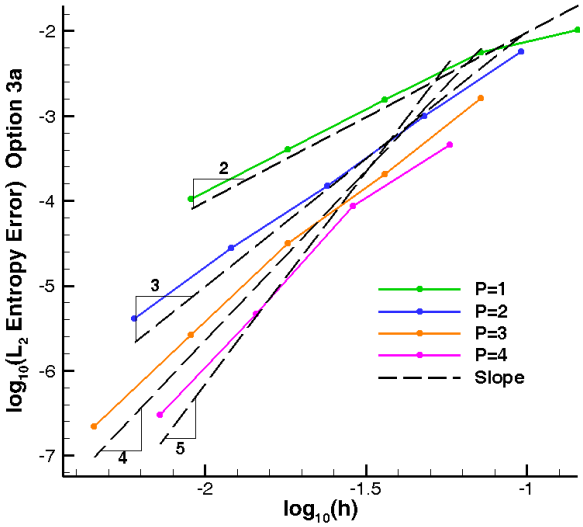

(b) Option 3a

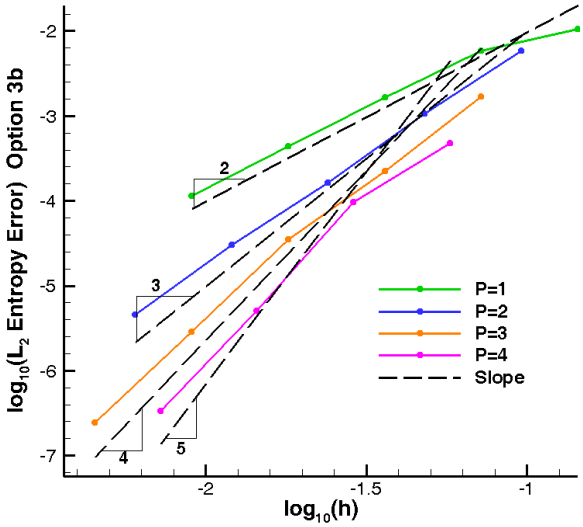

(c) Option 3b

Figure 2: H-Convergence for $N_g = 4$

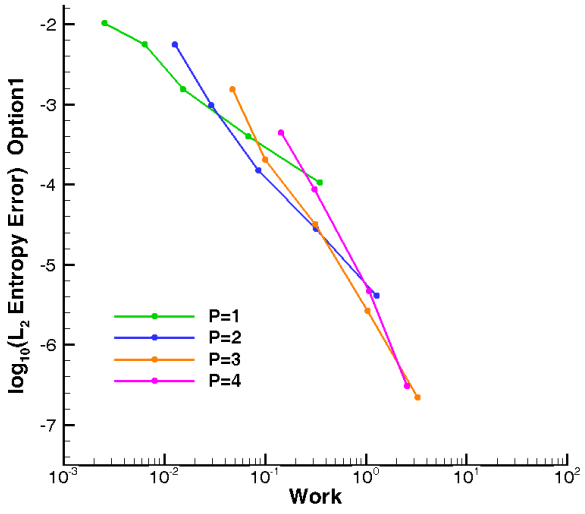

(a) Option 1

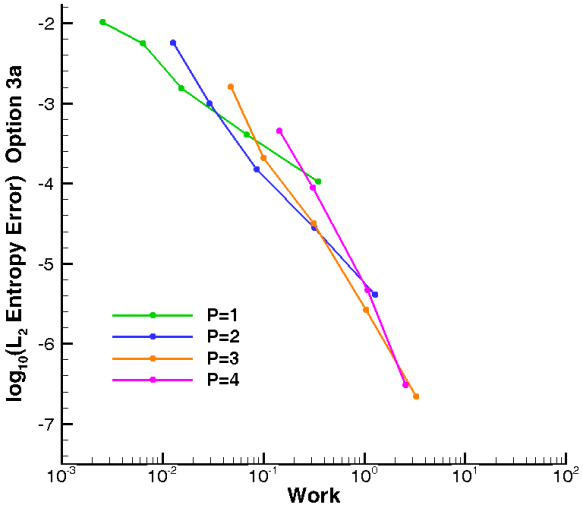

(b) Option 3a

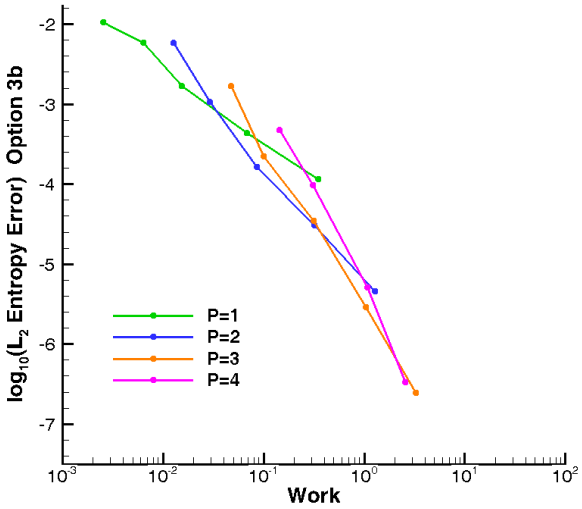

(c) Option 3b

Figure 3: Work for $N_g = 4$

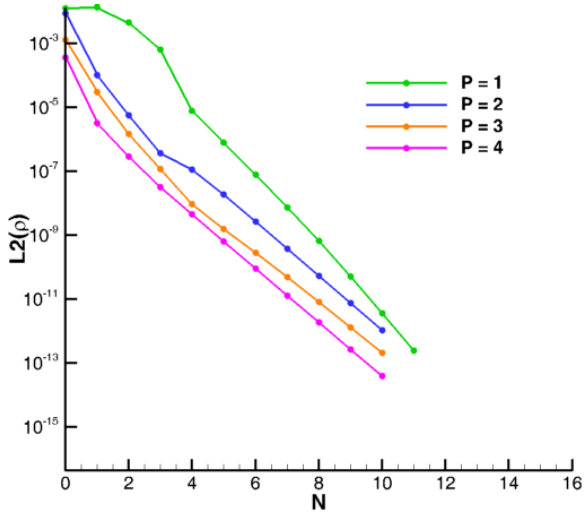

(a) 2x6

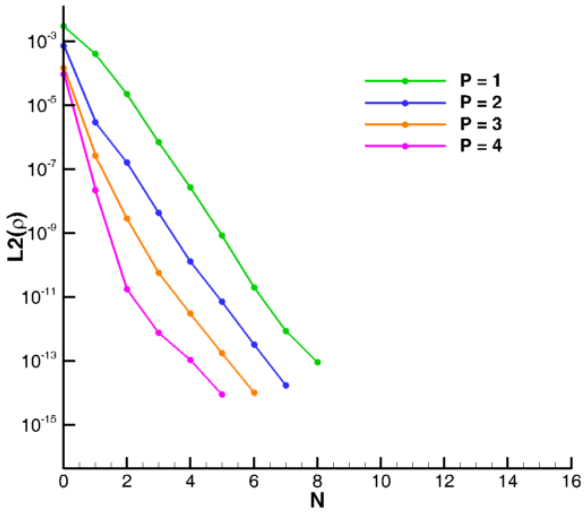

(b) 4x12

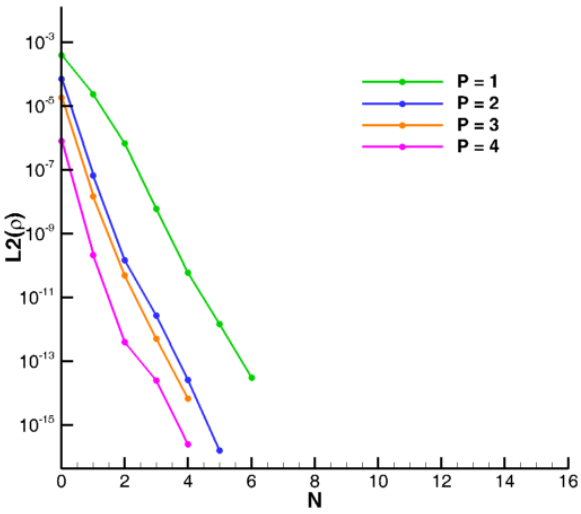

(c) 8x24

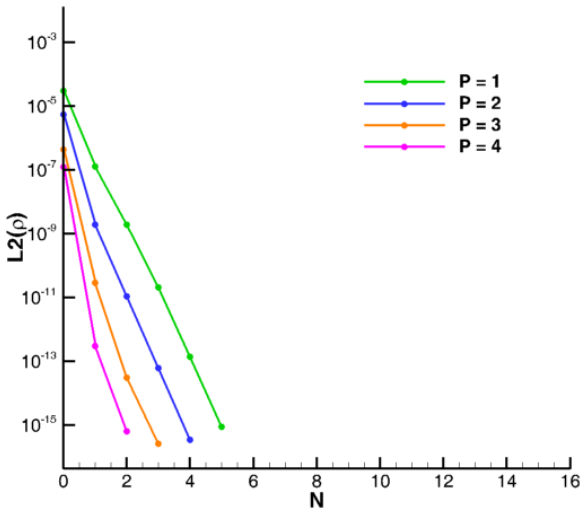

(d) 16x48

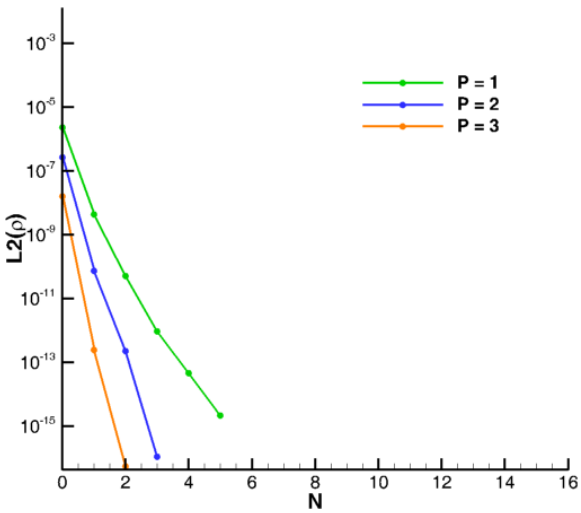

(e) 32x96

Figure 4: Newton Iteration Convergence History for $N_g = 4$

B. Slip Walls

Slip wall boundary conditions achieved similar results compared with imposing the Ringleb equations on the walls. However, the error tended to be slightly larger with slip walls, fewer simulations converged, and a pseudo-time step was required to achieve converged results. The results are shown in Figs. 5, 6 and 7.

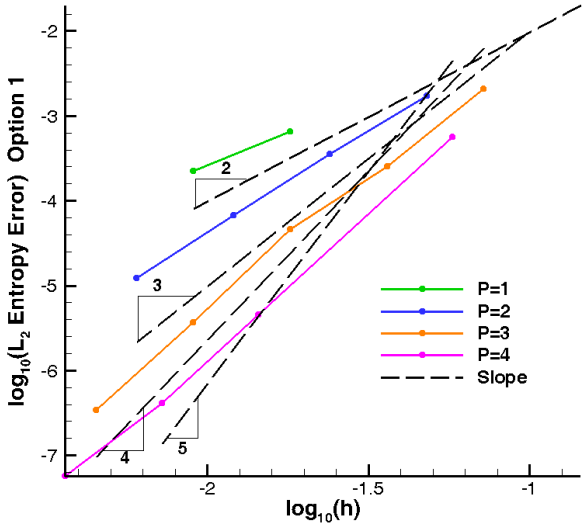

(a) Option 1

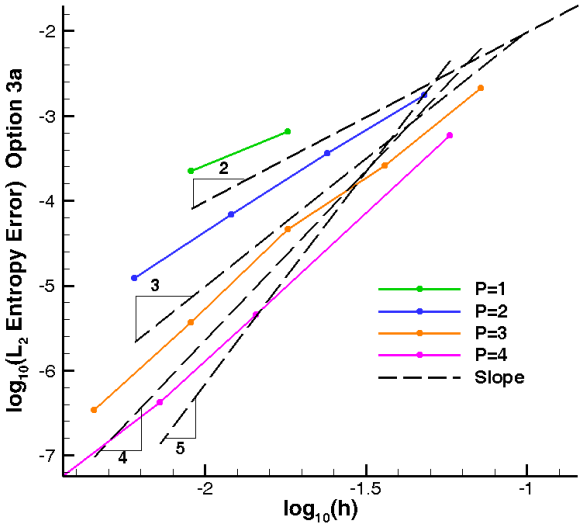

(b) Option 3a

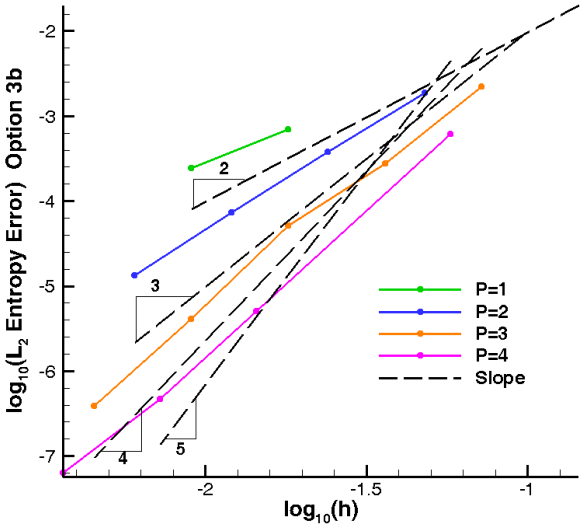

(c) Option 3b

Figure 5: H-Convergence for $N_g = 4$

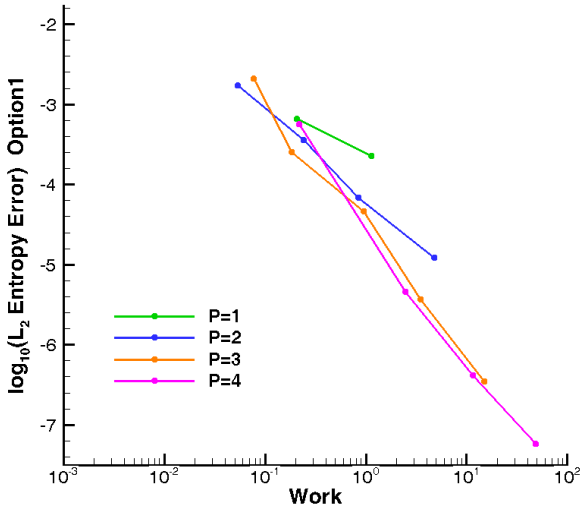

(a) Option 1

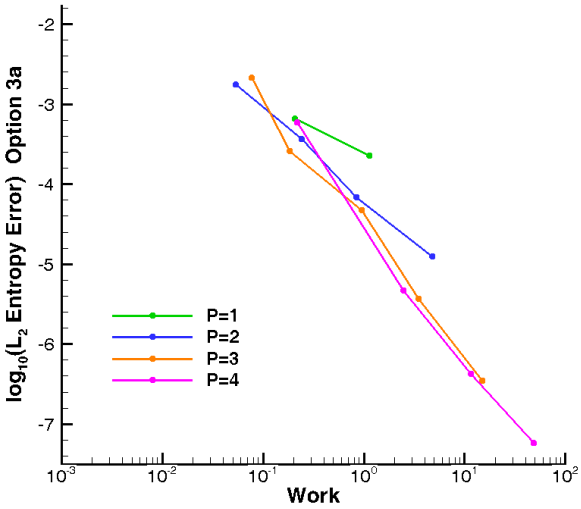

(b) Option 3a

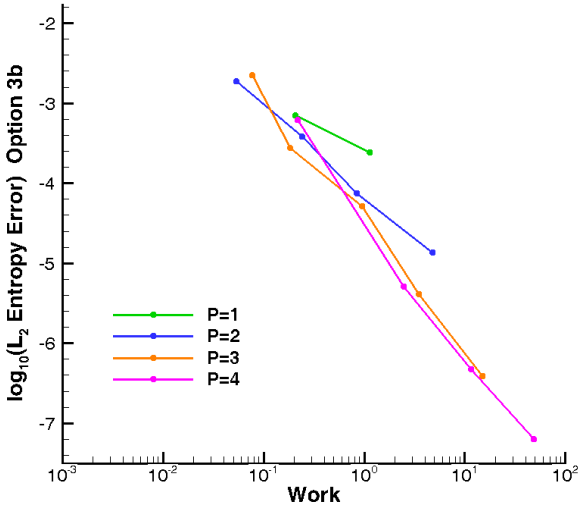

(c) Option 3b

Figure 6: Work for $N_g = 4$

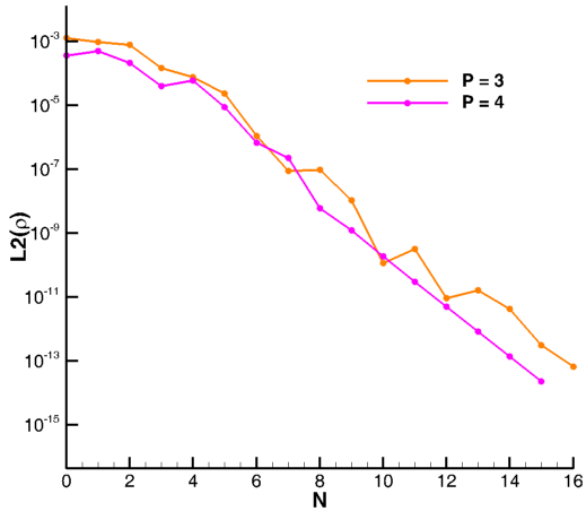

(a) 2x6

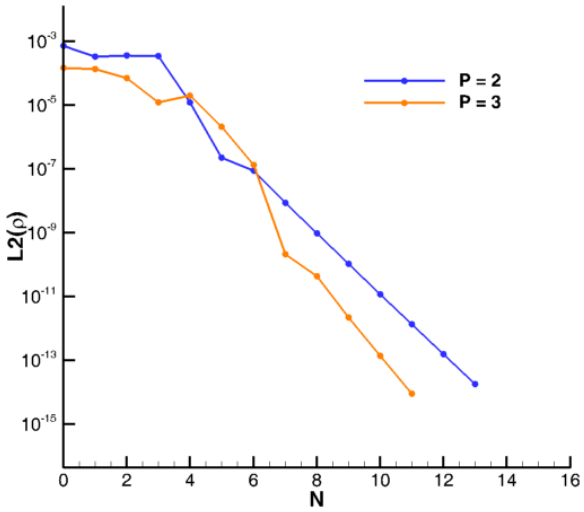

(b) 4x12

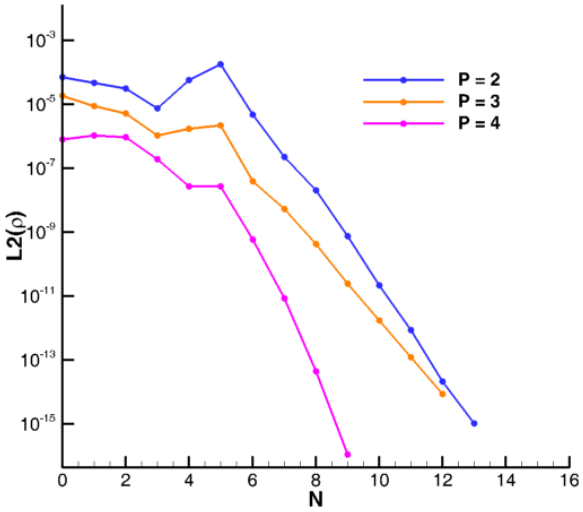

(c) 8x24

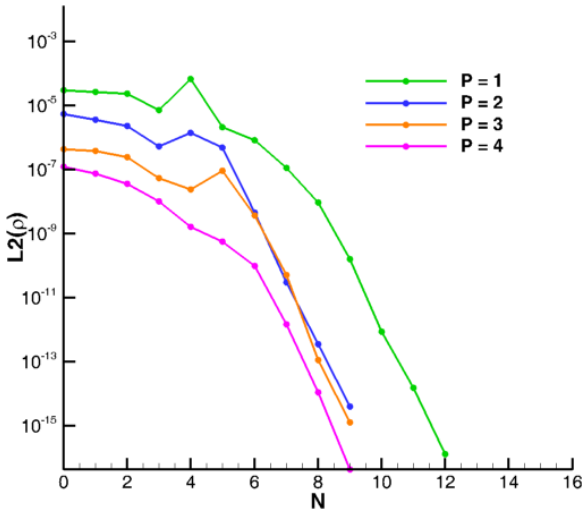

(d) 16x48

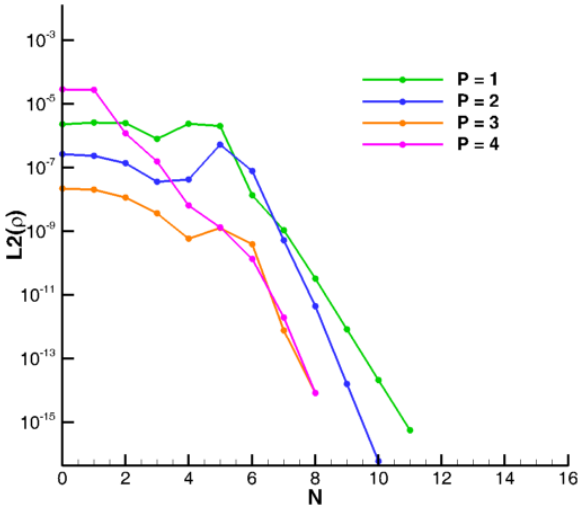

(e) 32x96

Figure 7: Newton Iteration Convergence History for $N_g = 4$

References

[1]Vatsa, V. N. and Wedan, J. L. T. B. W., "Navier-Stokes computations of prolate spheroids at angle of attack," AIAA-Paper 1987-2627, 1987.

[2]Galbraith, M. C., Orkwis, P. D., and Benek, J. A., "Automated Quadrature-free Discontinuous Galerkin Method Applied to Viscous Flows," AIAA-Paper 2011-493, 2011.

[3]Galbraith, M. C., Orkwis, P. D., and Benek, J. A., "Extending the Discontinuous Galerkin Scheme to the Chimera Overset Method," AIAA-Paper 2011-3409, 2011.

[4]Saad, Y., *Iterative methods for sparse linear systems*, SIAM, 2nd ed., 2000.